Finite-amplitude solitary waves at the interface between two homogeneous fluids

D. I. Pullin
Department of Mechanical Engineering, University of Queensland, St. Lucia, Queensland 4067, Australia
R. H. J. Grimshaw
School of Mathematics, University of New South Wales, P. O. Box 1, Kensington, New South Wales 2033, Australia

(Received 30 November 1987; accepted 9 August 1988)

Numerical solutions are presented for finite-amplitude interfacial waves. Only symmetric waves are calculated. Two cases are considered. In the first case the waves are free-surface solitary waves propagating on a basic flow with uniform vorticity. Large-amplitude waves of extreme form are calculated for a range of values of the basic vorticity. In the second case the waves are propagating on the interface between two homogeneous fluids of different densities, which are otherwise at rest. Again large-amplitude waves of extreme form are calculated for a range of values of the basic density ratio. In particular, in the Boussinesq limit when the density ratio is nearly unity, solitary waves of apparently unlimited amplitude can be found.

I. INTRODUCTION

It is well known that the free surface of a homogeneous fluid of finite depth supports solitary waves. When the elevation h of the wave crest above the depth d_1 of the undisturbed fluid at infinity is such that h/d_1 is very small, then these waves have a characteristic "sech^2" profile (see Miles[1] or Grimshaw[2] for recent reviews). As h/d_1 is increased, a limiting waveform is approached where $h/d_1 \approx 0.833\ 22$ (Hunter and Vanden-Broeck[3]), and for which the free surface exhibits a 120° corner at the crest. All members of this family of solitary waves exhibit an exponential decay in wave amplitude as the undisturbed fluid at infinity is approached (Stokes[4]).

In contrast to free-surface solitary waves, finite-amplitude solitary waves on the interface between two fluids, each of constant density $\rho_{1,2}$, have received comparatively little attention. For the case when each fluid has finite depth $d_{1,2}$ in the undisturbed fluid at infinity, solitary waves again have the characteristic "sech^2" profile when h/d_1 and h/d_2 are very small, and exhibit exponential behavior in the wave tails (Keulegan[5]). In contrast, if one of the fluids is infinitely deep (e.g., $d_2 \to \infty$ in Fig. 1), then it has been shown by Benjamin[6] and Davis and Acrivos[7] than when h/d_1 is very small, solitary waves are characterized by the form $h(1 + x^2/\lambda^2)^{-1}$, where λ is a measure of the width, and hence exhibit algebraic decay in the wave tails. When d_2 is large, but finite and comparable with λ, and h/d_1 is very small, solitary waves have a form intermediate between the "sech^2" profile and the algebraic form, but exhibit exponential decay in the wave tails (Joseph[8]). However, apart from various extensions of these small-amplitude theories to second order (see Grimshaw[2] for a recent review), little seems to be known about large-amplitude solitary waves. For the case when both fluids have finite depths $d_{1,2}$ in the disturbed fluid at infinity, Amick and Turner[9] have established the existence of finite-amplitude solitary waves which are supercritical, and waves of elevation or depression according as $\rho_2 d_1^2 \lesseqgtr \rho_1 d_2^2$. Here we say a wave is one of elevation (depression) if it faces into the upper (lower) fluid which has depth $d_1(d_2)$ at infinity. Interestingly this criterion is identical with that which holds for small-amplitude solitary waves. Further, Amick and Turner[9] showed that as the wave amplitude increases, either a vertical tangent must develop or the fluid system allows the formation of an internal bore. Recently Funakoshi and Oikawa[10] have reported numerical calculations of solitary waves for the case when $d_{1,2}$ are both finite, and found both families of solitary waves and internal bores. However, their method of calculation did not allow them to find solitary waves with vertical tangents or overhanging regions, if these exist.

In this paper we will describe the results of a study of numerical solutions for large-amplitude solitary waves on the interface between two fluids, each of constant density $\rho_{1,2}$ and constant vorticity $\omega_{1,2}$ with depths $d_{1,2}$ in the undisturbed field at infinity. Attention will be focused on two cases.

Case 1: Here $\rho_1 > 0, \rho_2 = 0, \omega_1$ is finite, and gravity g acts upwards (see Fig. 1). This corresponds to finite-amplitude solitary water waves in the presence of a uniform shear flow.

Case 2: (a) Here ρ_2 and ρ_1 are finite, $\rho_2 \neq \rho_1$, d_1 is finite but $d_2 \to \infty$, and $\omega_1 = \omega_2 = 0$. This configuration is for solitary interfacial waves with irrotational flow.

(b) This is the same as (a), but $\rho_1 \to \rho_2$ in the Boussinesq limit where the density difference is neglected in all but the buoyancy terms in the equations of motion and the boundary conditions.

Periodic interfacial waves have been extensively studied in

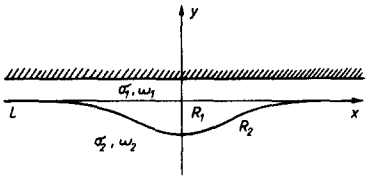

FIG. 1. The configuration in the Z plane ($Z = X + iY$) for solitary interfacial waves, in the case $D_1 \to \infty$. Here L is the wave profile, which is symmetric about $X = 0$, while L^m is the reflection of L in $Y = D_1$.

 0031-9171/88/123550-10$01.90

recent years (e.g., Simmen and Saffman,[11] and Teles da Silva and Peregrine[12] for free-surface waves on a shear flow; Holyer,[13] Vanden-Broeck,[14] Pullin and Grimshaw,[15,16] Meiron and Saffman,[17] Grimshaw and Pullin[18] and Turner and Vanden-Broeck[19] for interfacial waves between two fluids). These results show that large-amplitude waves occur with vertical tangents and overhanging regions. Our main aim here is to establish similar results for solitary waves.

II. EQUATIONS OF MOTION

In several recent papers (Pullin and Grimshaw[15,16] and Grimshaw and Pullin[18]) we studied periodic interfacial waves. The equations of motion are similar in this study of solitary waves, and hence we shall give just a brief description. The basic flow consists of two layers of inviscid incompressible fluids of densities $\rho_{1,2}$ and constant vorticity $\omega_{1,2}$ in plane parallel flow in the x direction. The y axis is normal to the undisturbed interface. The upper fluid lies in $0<y<d_1$ and is bounded above by a rigid plane $y=d_1$, while the lower fluid lies in $-d_2<y<0$ and is bounded below by a rigid plane $y=-d_2$. The unperturbed velocity field is then

$$\mathbf{u}_1=(-\omega_1 y,0),\quad 0<y<d_1\,, \tag{1a}$$

$$\mathbf{u}_2=(-\omega_2 y,0),\quad -d_2<y<0\,. \tag{1b}$$

Thus the interface $y=0$ is a discontinuity for density and vorticity. The gravity vector with magnitude $|g|$ acts parallel to the y axis and always points from the less dense into the more dense fluid, so that $g(\rho_2-\rho_1)>0$.

We shall view a solitary wave as an irrotational shape preserving perturbation to the basic flow that propagates with speed c. In a frame of reference at rest with respect to the wave, the streamfunction and velocity field in each fluid are given by

$$\psi_j'=-\tfrac{1}{2}\omega_j y^2-cy+\hat{\psi}_j,\quad j=1,2\,, \tag{2a}$$

$$u_j'=-\omega_j y-c+\hat{u}_j,\quad v_j'=\hat{v}_j,\quad j=1,2\,, \tag{2b}$$

where

$$\hat{u}_j=\frac{\partial\hat{\psi}_j}{\partial y}=\frac{\partial\hat{\phi}_j}{\partial x},\quad \hat{v}_j=-\frac{\partial\hat{\psi}_j}{\partial x}=\frac{\partial\hat{\phi}_j}{\partial y},\quad j=1,2\,. \tag{2c}$$

Here careted quantities are perturbation quantities in the laboratory frame of reference, and primed quantities are total quantities in the wave frame of reference. In the wave frame of reference the interface displacement from $y=0$ is denoted by $\eta(x)$. To describe a solitary wave we assume that

$$\eta(x)\to 0,\quad \psi_j'(x,\eta)\to 0\quad \text{as}\quad |x|\to\infty\,. \tag{3}$$

Next, since $y=\eta(x)$ must be a streamline of the flow, it follows that

$$\psi_1'(x,\eta)=\psi_2'(x,\eta)=0\,, \tag{4}$$

where the right-hand side is determined by considering the undisturbed flow as $|x|\to\infty$ (3). Further, $y=d_1,-d_2$ are also streamlines, and so

$$\psi_1'(x,d_1)=-cd_1-\tfrac{1}{2}\omega_1 d_1^2\,, \tag{5a}$$

$$\psi_1'(x,-d_2)=cd_2-\tfrac{1}{2}\omega_2 d_2^2\,. \tag{5b}$$

Note that in this formulation, the boundary conditions (4), (5a), and (5b) effectively exclude spatially periodic waves. Also, of course, $\hat{\psi}_{1,2}$ satisfies Laplace's equation in each fluid. Next we put $p_{1,2}=\hat{p}_{1,2}-\rho_{1,2}gy$, where $\hat{p}_{1,2}$ is the perturbation pressure, and require that $\hat{p}\to 0$ as $|x|\to\infty$. The Bernoulli equation is then

$$p_j/\rho_j+gy+\tfrac{1}{2}u_j'^2+\tfrac{1}{2}v_j'^2+\omega_j'\psi_j=\tfrac{1}{2}c^2\,,\quad j=1,2\,. \tag{6}$$

The remaining boundary conditions require that $p_1=p_2$ on $y=\eta$, or

$$\tfrac{1}{2}\rho_1(u_1'^2+v_1'^2-c^2)-\tfrac{1}{2}\rho_2(u_2'^2+v_2'^2-c^2)=(\rho_2-\rho_1)g\eta,\quad \text{on } y=\eta\,. \tag{7}$$

We shall conclude this section with a brief discussion of some of the integral properties of solitary waves, since the results are generally analogous to those for periodic waves (see Pullin and Grimshaw[15,16]). First, we define the "mass" to be

$$M=(\rho_2-\rho_1)A,\quad \text{where } A=\int_{-\infty}^{\infty}\eta\,dx\,, \tag{8}$$

and A is the area under the solitary wave profile. Next the excess impulse, or wave momentum, is defined by

$$I=\rho_2 Q_2+\rho_1 Q_1\,, \tag{9a}$$

where

$$Q_2=\int_{-\infty}^{\infty}\left(\int_{\eta}^{d_1}\hat{u}_1\,dy\right)dx+\frac{1}{2}\omega_1 A^{(2)}\,, \tag{9b}$$

$$Q_2=\int_{-\infty}^{\infty}\left(\int_{-d_2}^{\eta}\hat{u}_2\,dy\right)dx-\frac{1}{2}\omega_2 A^{(2)}\,, \tag{9c}$$

and

$$A^{(n)}=\int_{-\infty}^{\infty}\eta^n\,dx,\quad n=2,3,\ldots\,. \tag{9d}$$

It may now be shown that

$$Q_2=-Q_1=cA\,, \tag{10a}$$

and hence

$$I=cM\,. \tag{10b}$$

The excess kinetic and potential energies are now defined by

$$\begin{aligned}T=&\frac{1}{2}\rho_1\int_{-\infty}^{\infty}dx\left(\int_{\eta}^{d_1}(\hat{u}_1^2+\hat{v}_1^2)-2\hat{u}_1\omega_1 y\,dy\right)\\&-\tfrac{1}{6}\rho_1\omega_1^2A^{(3)}\\&+\frac{1}{2}\rho_2\int_{-\infty}^{\infty}dx\left(\int_{-d_2}^{\eta}(\hat{u}_2^2+\hat{v}_2^2)-2\hat{u}_2\omega_2 y\,dy\right)\\&+\tfrac{1}{6}\rho_2\omega_2^2A^{(3)}\,,\end{aligned} \tag{11a}$$

$$V=\tfrac{1}{2}g(\rho_2-\rho_1)A^{(2)}\,. \tag{11b}$$

It may now be shown that

$$\begin{aligned}2T=&c^2(\rho_2-\rho_1)A-\rho_1 d_1(c-\omega_1 d_1)C_1\\&-\rho_2 d_2(c-\omega_2 d_2)C_2+\tfrac{1}{2}c(\rho_2\omega_2-\rho_1\omega_1)A^{(2)}\\&+\tfrac{1}{3}(\rho_2\omega_2^2-\rho_1\omega_1^2)A^{(3)}+\rho_2\omega_2 H_2-\rho_1\omega_1 H_1\,,\end{aligned} \tag{12a}$$

where

$$C_j = [\hat{\phi}_j]_{-\infty}^{\infty}, \tag{12b}$$

and

$$H_j = \int_{-\infty}^{\infty} \hat{\phi}_j \eta \eta_x \, dx, \quad j = 1,2. \tag{12c}$$

Here C_j is the perturbation circulation in each fluid, and is a constant, while the integral in (12c) is along the interface. Further, it can be shown that

$$\pm d_j C_j = \int_{-\infty}^{\infty} \hat{\phi} \eta_x \, dx + cA + \frac{1}{2}\omega_j A^{(2)}, \quad j = 1,2, \tag{13}$$

where the integral in (13) is along the interface. Equation (13) shows that $d_2 C_2$ remains bounded as $d_2 \to \infty$. However, $d_2^2 C_2$ generally is unbounded as $d_2 \to \infty$, and hence the kinetic energy is unbounded as $d_2 \to \infty$ if $\omega_2 \neq 0$ [see (12a)]. Finally we note the relation

$$\begin{aligned} 3V = {} & [c^2(\rho_2 - \rho_1) - g(\rho_2 d_2 + \rho_1 d_1)]A \\ & - c(\rho_2\omega_2 - \rho_1\omega_1)A^{(2)} - \tfrac{4}{3}(\rho_2\omega_2^2 - \rho_1\omega_1^2)A^{(3)} \\ & + \rho_2\omega_2 d_2^2 C_2 + \rho_1\omega_1 d_1^2 C_1 - (d_1 + d_2)\int_{-\infty}^{\infty} p_L \, dx, \end{aligned} \tag{14}$$

where p_L is the pressure on the interface, and it can be shown that

$$\int_{-\infty}^{\infty} p_L \, dx = -g\rho_j A + \int_{-\infty}^{\infty} (p + g\rho_j y)_{y = d_1, d_2} \, dx, \quad j = 1,2. \tag{15}$$

For free-surface solitary waves (i.e., $\rho_1 = 0$ or $\rho_2 = 0$), and in the absence of any vorticity (i.e., $\omega_2 = 0$ or $\omega_1 = 0$), these results agree with those described by Longuet-Higgins.[20] They are derived using similar techniques.

III. INTEGRAL EQUATION FORMULATION

We now introduce dimensionless variables by choosing a length scale H and a time scale $(H/\alpha g)^{1/2}$, where $\alpha = (\rho_2 - \rho_1)/(\rho_2 + \rho_1)$ is the Boussinesq parameter, with the range $-1 \leqslant \alpha < 1$. Since the gravity vector always points into the more dense fluid, we must have $\alpha g > 0$. We will generally take $H = d_1$, so that the nondimensional depth $D_1 = 1$ in the subsequent development, but in one limiting case we will choose H to be a multiple of wave amplitude, and this will be indicated in the appropriate context. We next introduce the dimensionless variables $(X, Y, D_j, \Omega_j, U_j, V_j, \Psi_j, Y_c, C, A)$ which are equivalent to the dimensional variables $(x, y, d_j, \omega_j, u_j', v_j', \psi_j', \eta, c, h)$, where A now denotes the dimensionless amplitude. In terms of these variables the boundary conditions (4) and (7) become

$$\Psi_1 = \Psi_2 = 0, \quad \text{on } Y = Y_c, \tag{16a}$$

$$\begin{aligned} & (1-\alpha)(U_1^2 + V_1^2 - C^2) - (1+\alpha)(U_2^2 + V_2^2 - C^2) \\ & \quad = 4Y_c, \quad \text{on } Y = Y_c. \end{aligned} \tag{16b}$$

The free-surface solitary wave is recovered by putting $\alpha = -1$, in which case gravity points in the positive Y direction. When $\alpha = 0$ we obtain the Boussinesq limit, for which it may be shown that gravity can point in either the positive or negative Y direction for the same wave profile. For all the numerical results reported here, we let $D_2 \to \infty$ and put $\Omega_2 = 0$.

A. Conformal mapping

In terms of the complex coordinate $Z = X + iY$, we describe the interface profile by

$$Z_c(a) = X_c(a) + iY_c(a), \quad -\pi \leqslant a \leqslant \pi, \tag{17a}$$

where

$$X_c \to \pm\infty, \quad Y_c \to 0, \quad \text{as } a \to \pm\pi. \tag{17b}$$

Here a denotes a parameter that will be specified subsequently. We shall restrict attention to solitary waves that are symmetrical about $X = 0$. We do not assert that solitary waves are necessarily symmetrical, but it seems likely that if nonsymmetrical solutions exist, they will appear through bifurcation off solution branches of symmetrical waves (e.g., see Zufiria[21,22] for a study of nonsymmetric spatially periodic free-surface waves). The possible existence of nonsymmetric waves will be left for future study, although we note that Zufiria[23] has shown that there are nonsymmetric free-surface gravity–capillary solitary waves.

The symmetrical solutions may be selected by choosing $X_c(0) = 0$, and by requiring that

$$Z_c(-a) = -Z_c^*(a). \tag{18}$$

Letting $D_2 \to \infty$, the configuration for the symmetrical solitary wave is shown in Fig. 1, in which L is the interfacial profile. We define L^m as the reflection of L in $Y = D_1$. The region bounded by L and $Y = D_1$ is denoted by R_1, and that below L by R_2. Also R_j^m is the reflection of R_j in $Y = D_1$ for $j = 1,2$.

At this point we mention a potential difficulty in calculating numerically solitary interfacial waves; this is the treatment of the wave tails. When $\alpha = -1$ (or when D_2 is finite), an argument based on local solutions of Laplace's equation in the tail region may be used to show that the tail decays exponentially (Stokes[4]). However, when $D_2 \to \infty$, such local arguments fail because of the infinite inertia of the fluid in R_2. Although it is likely that the tail decays algebraically as X^{-2}, the wave tail is not known at the outset, and must be determined as part of the overall solution. In order to incorporate a self-consistent treatment of the full wave profile, including the tail, we introduce a conformal mapping to the ζ plane ($\zeta = \xi + i\eta$) given by, when $D_1 = 1$,

$$\zeta = -Z/(Z - 2i). \tag{19}$$

This maps the half-planes $-\infty < Y \leqslant 1$ and $1 < Y < \infty$ into the interior and exterior, respectively, of the circle $|\zeta| = 1$; the lower half-plane $Y \leqslant 0$ is mapped into the interior of the circle $|\zeta + \frac{1}{2}| = \frac{1}{2}$, and $Z = \infty$ is mapped into $\zeta = -1$. If we form a closed anticlockwise running curve in the Z plane made up of L and L^m and closed by straight vertical lines at $X = \pm\infty$, then the image of this curve in the ζ plane is the closed clockwise running curve comprising $\mathscr{L}$ (the image of

L) and $\mathscr{L}^m$. Also (19) maps R_j and R_j^m into $\mathscr{R}_j$ and $\mathscr{R}_j^m$, respectively. In the ζ plane $\mathscr{L}$ is specified by

$$\zeta_c(a) = \xi_c(a) + i\eta_c(a), \tag{20a}$$

where

$$\zeta_c \to -(1 \pm 0i) \quad \text{as} \quad a \to \pm\pi. \tag{20b}$$

The symmetry condition (18) becomes

$$\zeta_c(-a) = \zeta^*(a). \tag{21}$$

Next we must consider the specification of Ψ_j, U_j, and V_j so that the boundary conditions can be satisfied on L or $\mathscr{L}$. The different features of solitary waves when $\alpha = -1$ and when $\alpha > -1$ lead to different, but overlapping, methods of parametrizing the interface. We consider the case $\alpha = -1$ first.

B. Parametrization: $\alpha = -1$

In this case we need only deal with the flow in R_1 of Fig. 1. We parametrize L using the method of Simmen and Saffman[11] for periodic free-surface waves, adapted here for solitary waves. First, by Cauchy's integral theorem, the complex velocity $U - iV$ at the point $Z = X + iY$ in R_1 is given by

$$U_1 - iV_1 = -\frac{1}{2\pi i}\oint_{L+L^m} \frac{(\hat{U}_1 - i\hat{V}_1)_c\, dz'}{(Z - Z')} - \Omega_1 Y - C, \tag{22}$$

where $\hat{U} - i\hat{V}$ is the dimensionless perturbation velocity at Z, and the integral is taken over L and L^m. When Z_c is on L^m, $\hat{U}_1 - i\hat{V}_1$ is interpreted as the complex conjugate of the velocity at the reflection point on L. It follows that the boundary condition on $Y = 1$ is automatically satisfied. Next we let $Z \to Z_c$ from above, and write $U_1 - iV_1 = Q_1\, ds/dZ_c$, where Q_1 is the fluid speed on the free surface L, and s is the arclength on L. Then (2b) shows that

$$Q_1 \frac{ds}{dZ_c} = \hat{U}_1 - i\hat{V}_1 - \Omega_1 Y_c - C. \tag{23}$$

Now on L,

$$\frac{ds}{dz_c} = \frac{ds}{d\sigma}\frac{d\sigma}{da}\frac{da}{dz_c} = \left|\frac{ds}{d\zeta}\right|_c \frac{d\sigma}{da}\frac{da}{dZ_c}, \tag{24}$$

where σ is the arclength on $\mathscr{L}$. Using (23) and (24),

$$(\hat{U}_1 - i\hat{V}_1)_c = Q_1 \frac{d\sigma}{da}\left|\frac{dZ}{d\zeta}\right|_c \frac{da}{dZ_c} + \Omega_1 Y_c + C. \tag{25}$$

The parameter a is now defined by putting

$$\frac{d\sigma}{da} = -MQ_1(1 - \beta\cos a), \tag{26}$$

where m is an unknown constant and β ($-1 < \beta < 1$) is a specified constant. We shall call (26) the Q_1 parametrization. Substituting (26) into (25), eliminating Q_1^2 using (16b) (for $\alpha = -1$), and using the resulting expression for $(\hat{U}_1 - i\hat{V}_1)_c$ in (22), then gives

$$U_1 - iV_1 = \frac{1}{2\pi i}\oint_{L+L^m} \frac{F(a')da'}{(Z - Z')} - \Omega_1 Y - C, \tag{27a}$$

where

$$F(a) = M(2Y_c + C^2)(1 - \beta\cos a)\left|\frac{dZ}{d\zeta}\right|_c - (\Omega_1 Y_c + C)\left(\frac{dZ}{d\zeta}\frac{d\zeta}{da}\right)_c. \tag{27b}$$

When $a \to \pm\pi$ in the wave tails, it can be seen from (19) that $dZ/d\zeta$ is singular, so that F is then the difference between two singular terms. However, it may be shown from the exponential decay of Y_c for large $|X|$ that $F(a) \to 0$ as $a \to \pm\pi$. Equations (27a) and (27b) express $U_1 - iV_1$ entirely in terms of $Z_c(a)$. The streamfunction is readily obtained from (27a) and is given by

$$\Psi_1 = \mathrm{Im}\left(\frac{1}{2\pi i}\oint_{L+L^m} \log(Z - Z')F(a')da'\right) - \tfrac{1}{2}\Omega_1 Y^2 - CY. \tag{28}$$

For numerical convenience we work in the ζ plane. This introduces a singularity at $\zeta = -1$, but allows terms such as dZ_c/da to become singular in a known way when $a \to \pm\pi$. Using (19) we find that (27a) and (28) become

$$U_1 - iV_1 = \frac{(1+\zeta)}{2\pi i} \times \oint_{\mathscr{L}+\mathscr{L}^m} \frac{(1+\zeta')F(a')da'}{2i(\zeta - \zeta')} - \Omega_1 Y - C, \tag{29a}$$

$$\Psi = \mathrm{Im}\left(\frac{1}{2\pi i}\oint_{\mathscr{L}+\mathscr{L}^m} [\log(\zeta - \zeta') - \log(-1 - \zeta')]F(a')da'\right) - \tfrac{1}{2}\Omega_1 Y^2 - CY, \tag{29b}$$

where, in obtaining (29b), we have used (3) to determine a constant. Using (29a) and (29b) in (16a) and (16b) leads, together with (21), to two coupled nonlinear integrodifferential equations for the complex-valued function $\zeta_c(a)$, $-\pi \leqslant a \leqslant \pi$. There are two unknown constants C and M, and these must be determined as part of the solution. The parametrization (26) automatically concentrates points near the wave crest for large amplitude waves, when we expect the wave profile to form a 120° corner at the crest and $Q_1 \to 0$. The term $(1 - \beta\cos a)$ in (26), with β specified, allows further control of the distribution of points near $\zeta = -1$.

C. Parametrization: $-1 \leqslant \alpha < 1$

The choice of interface parametrization is constrained by two requirements. One is that ds/da (or $d\sigma/da$) be monotonic on L, which ensures that a is single valued. A second requirement is that a be finite valued when $|X_c| \to \infty$. For $\alpha = -1$, we do not expect Q_1 to change sign on $\mathscr{L}$, and, since $\mathscr{L}$ has finite length, Eq. (26) ensures that both of these requirements are satisfied. But when $\alpha > -1$, we must also consider the fluid in R_2 (see Fig. 1). Unfortunately for $\alpha > -1$, we have been unable to generalize (26), and continue to satisfy the parametrization requirements. The natu-

ral choice, which would replace Q_1 in (26) with $[(1-\alpha)Q_1^2-(1+\alpha)Q_2^2]/(Q_1-Q_2)$ was tried, but found to give a change of sign in $d\sigma/da$ for some values of α. Hence, for $-1\leqslant\alpha<1$, we have modified the arclength parametrization used by Pullin and Grimshaw[15,16] for periodic waves to suit the present case. Thus we introduce a real-valued vortex/source singularity distribution on L, with strength $\gamma(a)$, and replace (27a) and (27b) with

$$U_j-iV_j=\frac{1}{2\pi i}\oint_{L+L^m}\frac{G(a')da'}{Z-Z'}-\Omega_j Y-C, \quad (30a)$$

where

$$G(a)=\gamma(a)+i\Delta\Omega Y_C\frac{dY_c}{da}. \quad (30b)$$

Here $j=1,2$ refers to Z lying in R_j and $\Delta\Omega=\Omega_2-\Omega_1$. It is readily shown that $\gamma\,da/ds$ is the local jump in the perturbation tangential velocity across L and that $\gamma\to 0$ as $a\to\pm\pi$. Also, it may be shown that $\int_L\gamma\,da$ is bounded, and that the integral term in (30a) is asymptotically zero when $Z\to\infty$; hence U_j-iV_j approaches the unperturbed flow in this limit. We again note that when Z' is on L^m, the corresponding G is the complex conjugate of (30b) applied at the reflection point on L. Hence the boundary condition on $Y=1$ is automatically satisfied.

In the ζ plane, the equivalents of (29a) and (29b) are

$$U_j-iV_j=\frac{(1+\zeta)}{2\pi i}\oint_{\mathscr{L}+\mathscr{L}^m}\frac{(1+\zeta')G(a')da'}{2i(\zeta-\zeta')}-\Omega_j Y-C, \quad (31a)$$

$$\Psi_j=\mathrm{Im}\left(\frac{1}{2\pi i}\oint_{\mathscr{L}+\mathscr{L}^m}[\log(\zeta-\zeta')-\log(-1-\zeta')]G(a')da'\right)-\tfrac{1}{2}\Omega_j Y^2-CY. \quad (31b)$$

When $\zeta\to\zeta_c$ from either side of $\mathscr{L}$ and (31a) and (31b) are used in (16a) and (16b), we again obtain coupled integro-differential equations, but there is now an extra unknown, $\gamma(a)$. The closure equations are obtained by defining a as follows:

$$\frac{d\sigma}{da}=M(1-\beta\cos a), \quad (32)$$

where again M is an unknown constant, and β is a specified constant. We refer to (32) as the σ parametrization.

We note that using Ψ to satisfy the kinematic boundary condition will lead to additional computation, which may in principle be avoided by replacing (16a) with the equivalent condition that the normal velocity on L, $\partial\Psi/\partial s$, is zero. However, this has two disadvantages. First, it does not automatically select the solitary wave solution from, say, X-wise periodic solutions; this must then be enforced using additional constraints. Second, implementation of $\partial\Psi/\partial s$ being zero on L introduces terms like $\mathrm{Re}[(U-iV)dZ_c/da]$, which in the wave tail contain the product of asymptotically small and asymptotically singular terms. This is likely to produce severely ill-conditioned equations in the numerical discretization, and in fact this was found to be the case when this alternative formulation was tested.

IV. NUMERICAL METHOD

For the numerical method we choose a finite-difference formulation in preference to a spectral technique, since the former is better able to handle severe profile deformations such as overhanging portions, and the very high profile curvature associated with the incipient formation of a sharp corner. The general approach is similar for both the Q_1 and σ parametrizations, although we shall note essential differences where appropriate.

Calculations were carried out, for the most part, in the ζ plane. The contour $\mathscr{L}$ is defined for numerical purposes by $2N$ points $\zeta_n=\xi_n+i\eta_n$, $n=-N,\ldots,N$, with $\zeta_{\pm N}=(1\pm 0i)$ and $\zeta_0=\xi_0$. Note that now and subsequently, for convenience, we omit the c subscript when ζ is on $\mathscr{L}$. In the Z plane, the equivalent points on L are Z_n, $n=-N,\ldots,N$ given by (19), $Z_{\pm N}=\pm\infty$, and $Z_0=0-iA$, where A is a measure of wave amplitude. Corresponding to these sets of points are the discretized, equispaced values of a given by $a_n=n\pi/N$, $n=-N,\ldots,N$. The symmetry condition (21) is enforced by requiring that $\zeta_{-n}=\zeta_n^*$, $n=0,\ldots,N$, and $\mathscr{L}^m$ is defined by the points $1/\zeta_n^*$, $n=-N,\ldots,N$. With the Q_1 parametrization the unknowns are the $2N+1$ quantities (ξ_n,η_n) $[n=-(N-1),\ldots,-1]$, ξ_0, C, and M. With σ parametrization there are N extra unknowns γ_n, $n=-(N-1),0$ $(\gamma_{-n}=\gamma_n)$, which are the discrete values of $\gamma(a)$ for $a=n\pi/N$. We denote either this $(2N+1)$- or $(3N+1)$-tuple of unknowns by $\mathbf{w}$.

The boundary conditions were implemented by satisfying (16a) and (16b) at each of the points ζ_n, $n=-(N-1),\ldots,0$, giving $2N$ real nonlinear equations. The singular integrals that occur in (29a) and (29b), say, when ζ approaches a point ζ_n from either side of $\mathscr{L}$, were treated numerically by first subtracting out the respective singularities, and then applying the periodic trapezoidal rule to the remaining integrals (see Pullin and Grimshaw[15,16] for more details of this technique). We note that when the wave tail decays algebraically, which we expect to occur for $\alpha>-1$, G may suffer discontinuities in derivative when $a\to\pm\pi$, and then the periodic trapezoidal rule will not give formal infinite-order accuracy. All derivatives with respect to a up to second order on $\mathscr{L}$ were calculated using a five-point finite difference rule.

When $\alpha=-1$, the boundary conditions together with the Q_1 parametrization give $2N$ equations for the $2N+1$ unknowns. The closure equation was supplied by implementing pseudoarclength continuation (Keller[24]). Briefly, let $\mathbf{w}(\delta)$ represent a solution point on a smooth branch in the $(2N+1)$ space defined by $\mathbf{w}$ where δ is the pseudoarclength defined by

$$\frac{1}{2}\left|\left|\frac{\partial\mathbf{w}}{\partial\delta}\right|\right|-1=0, \quad (33)$$

and $\| \ \|$ refers to an appropriate norm. If $\mathbf{w}(\delta_{k-1})$ is the $(k-1)$th discrete solution point obtained on the branch, then the solution at δ_k is sought by closing the system of nonlinear equations using

$$\tfrac{1}{2}\|\mathbf{w}(\delta_k) - \mathbf{w}(\delta_{k-1})\|^2 - (\delta_k - \delta_{k-1})^2 = 0 . \quad (34)$$

Thus δ takes the role of an independent parameter, and *all* physically significant parameters are determined as part of each particular numerical solution. Pseudoarclength continuation easily detects turning point behavior, and may be adapted to search for bifurcations off a known solution branch: We note that there may be nonuniqueness of solutions using pseudoarclength continuation near a bifurcation point, but we found no indication of related difficulties (e.g., vanishing of the Jacobian) for the computations reported presently. The $2N+1$ nonlinear equations were solved using Newton–Raphson iteration in 14-figure arithmetic. The Jacobian was evaluated by two-point one-sided finite differences in $\mathbf{w}$ space, giving an overall computation time of $O(N^3)$.

When $\alpha > -1$, the σ parametrization introduces N new unknowns γ_n, $n = -(N-1),...,0$ (note that $\gamma_{-n} = 0$). The extra N closure equations are a discretized version of (32),

$$|\zeta_n - \zeta_{n-1}| - (M\pi/N)\left[1 - \tfrac{1}{2}\beta(\cos a_n - \cos a_{n-1})\right] = 0 ,$$
$$n = -(N-1),...,0 . \quad (35)$$

We note that the low-order approximation of (32) does not affect the solution accuracy. We have merely replaced the continuous definition of σ by a chord-length based parametrization. These are now $3N+1$ nonlinear equations for $3N+1$ unknowns, and hence the σ parametrization is substantially more expensive than the Q_1 parametrization.

The present formulation was tested by calculating properties of free-surface irrotational solitary waves ($\alpha = -1$, $\Omega_1 = 0$), and comparing our results with the accurate calculations of Hunter and Vanden-Broeck[3] and Tanaka.[25] Table I shows a comparison of our predicted values of C for very large-amplitude waves with the results of Tanaka, who used the fluid speed at the wave crest ($Q_c = Q_1$ at $X = 0$) as an independent parameter. With $N = 40$, the Q_1 parametrization gives four-figure accuracy compared with Tanaka's results, up to the first minimum in C (as a function of Q_c). The Q_1 parametrization gives progressively poorer results as Q_c reduces, presumably because the scheme begins to fail for wave profiles very near the limiting wave, where dZ_c/da suffers a discontinuity at the 120° corner. With $Q_c = 0.04$, $N = 40$ we find $A = 0.834\,12$ compared to the limiting wave amplitude $A = 0.833\,22$ obtained by Hunter and Vanden-Broeck.[3]

TABLE I. Wave speed C versus the fluid speed at the crest Q_c, for free-surface irrotational solitary waves ($\alpha = -1$, $\Omega_1 = \Omega_2 = 0$). (a) The results of Tanaka[25]; (b) the results from the Q_1 parametrization scheme, $N = 40$; (c) the results from the Q_1 parametrization scheme, $N = 20$; (d) the results from the σ parametrization scheme, $N = 40$.

Q_c	(a) C	(b) C	(c) C	(d) C
0.250	1.293 85	1.293 96	1.294 30	1.293 17
0.200	1.294 01	1.293 87	1.293 22	1.292 35
0.150	1.292 64	1.291 69	1.292 27	1.291 04
0.100	1.291 27	1.291 03	1.292 27	1.288 47
0.080	1.290 98	1.290 96	1.292 09	1.287 85
0.060	1.290 86	1.290 98	⋯	1.287 85
0.040	1.290 86	1.290 99	⋯	1.287 85

V. RESULTS AND DISCUSSION

A. Free-surface solitary waves on a uniform shear flow: $\alpha = -1$

With $\alpha = -1$, computations were performed with $N = 40$ or 80, using both the Q_1 and σ_1 parametrization with $-1.1125 \leqslant \Omega_1 < 0.5$. Numerical solutions were obtained along branches corresponding to fixed values of Ω_1. A starting guess was provided by an approximate solution valid for small amplitudes ($A = h/d_1 \ll 1$). In dimensional variables this is given by the familiar "sech²" profile, described here by

$$y = -h\,\mathrm{sech}^2(x/\lambda) , \quad (36a)$$

where

$$h\lambda^2 = 12\Delta/\mu, \quad c = c_0 + \tfrac{1}{3}\mu h , \quad (36b)$$

and

$$c_0 = -\tfrac{1}{2}\omega_1 d_1 + (\tfrac{1}{4}\omega_1^2 d_1^2 + g d_1)^{1/2} , \quad (36c)$$
$$\mu = (3g d_1 + \omega_1^2 d_1^2)/2d_1(\tfrac{1}{4}\omega_1^2 d_1^2 + g d_1)^{1/2} , \quad (36d)$$
$$\Delta = d_1^2 c_0^2/6(\tfrac{1}{4}\omega_1^2 d_1^2 + g d_1)^{1/2} . \quad (36e)$$

A sequence of solutions was then found on the branch, $\Omega_1 = \text{const}$, by incrementing δ and, at each step, using as an initial approximation an estimate obtained by extrapolation from previously obtained solutions on the $\mathbf{w}(\delta)$ arc. This process was terminated when either several successive halvings of the increment in δ failed to produce a new converged solution, or, as occurred in some instances, difficulties in obtaining the required accuracy appeared. These usually appeared in the form of either insufficient smoothness in the wave profile, or of incorrect asymptotic behavior in the wave tail owing to insufficient resolution.

In Fig. 2 we depict graphs of speed C versus amplitude A for branches with constant Ω_1. When $-0.75 \leqslant \Omega_1 \leqslant 0.5$, the

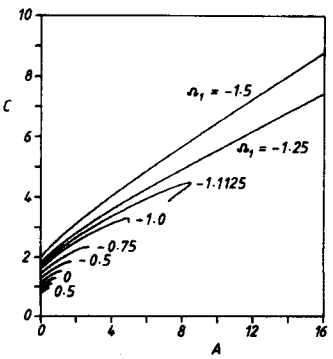

FIG. 2. Wave speed C versus wave amplitude A for free-surface solitary waves on a uniform shear flow; $\alpha = -1$, and values of Ω_1 indicated.

graphs are qualitatively similar to those for $\Omega_1 = 0$; $C - C_0$ [C_0 is the nondimensional value of c_0 in (36c)] is proportional to A for $A \ll 1$, followed by a monotonic decrease in $\partial C/\partial A$ as A increases to a maximum value of C, followed in turn by small-scale oscillations as a limiting profile with a 120° corner at the crest is approached. For this range of Ω_1 we believe our results are reliable to the values of A that lie between the first minimum and the second maximum in C. The computed extreme wave profiles with $-1.125 \leqslant \Omega_1 \leqslant 0.5$ are shown in Fig. 3, where by "extreme wave" with amplitude A_{ex} we mean the numerical solution with the largest value of δ on a particular $\mathbf{w}(\delta)$ arc that could be reliably obtained with the present numerical methods. Values of A_{ex} are given in Table II. Note that A_{ex} is not necessarily the maximum wave amplitude. These extreme waves should be distinguished from the limiting waves, which are the conjectured wave profiles with a 120° corner at the crest, and which presumably occur at the end of a $\mathbf{w}(\delta)$ branch. Evaluating the Bernoulli relation (16b) at the wave crest of a limiting wave where $Q_1 = 0$, it follows that

$$\tfrac{1}{2}C_{\lim}^2 = A_{\lim}, \tag{37}$$

and values of $\frac{1}{2}C^2$ corresponding to A_{ex} are also shown in Table II.

Our results shown in Figs. 2 and 3 indicate that $A_{\lim}$ increases as $-\Omega_1$ increases, and that limiting waves of very large amplitude are possible when $\Omega_1 Y$ and C have the same sign near the wave crest (here $Y<0$, $\Omega_1<0$, and $C>0$). Thus, for instance, when $\Omega_1 = -1$ [or $\omega_1 = -(g/d_1)^{1/2}$ in dimensional variables], there is a sixfold increase in the maximum allowable amplitude, compared to free-surface solitary waves in the absence of shear ($\Omega_1 = 0$). Some insight into the reasons for this can be obtained by considering the relations (36) and (37). Thus (36c) shows that C_0 increases as $-\Omega_1$ increases, and from (36b) and (36d) we expect C to increase with A for each fixed Ω_1, at least initially. It could then be inferred from (37) that $A_{\lim}$ should increase as $-\Omega_1$ increases. These observations are in agreement with the trends shown in Figs. 2 and 3.

The small-amplitude relations may be used to provide some insight into the possible existence of solutions that scale on $h_{\lim}$ when Ω_1 is large and positive, since the numerical results show that $A_{\lim}$ decreases rapidly as Ω_1 increases.

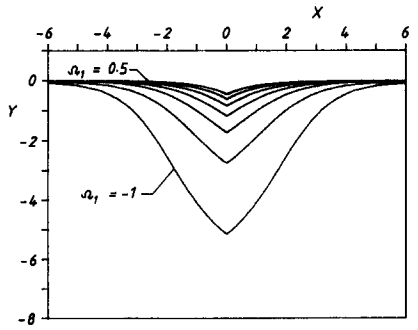

FIG. 3. Extreme wave profiles for free-surface solitary waves on a uniform shear flow; $\alpha = -1$, $0.5 > \Omega_1 > -1.0$. Here gravity acts in the positive Y direction.

TABLE II. The amplitude A_{ex} of the extreme waves versus Ω_1. For the conjectured limiting wave with a 120° corner at the wave crest, $A_{\lim} = \frac{1}{2}C_{\lim}^2$. The results for $\Omega_1 = -1.1125$ were performed with the σ parametrization, and we were unable to approach close to the limiting wave solution.

Ω_1	A_{ex}	$\frac{1}{2}C_{ex}^2$
0.5	0.458 99	0.458 99
0.25	0.611 50	0.611 59
0	0.834 12	0.834 22
−0.25	1.169 6	1.169 56
−0.50	1.792 8	1.793 1
−0.75	2.715 3	2.726 3
−1.0	5.137 8	5.138 8
−1.1125	7.490 3	7.958 6

Equations (36) and (37) may be used to estimate $A_{\lim}$ (or $h_{\lim}$ in dimensional variables) and $\lambda_{\lim}$ for $\Omega_1 \gg 1$. We find that $h_{\lim} \sim 18g/\omega_1^2$ and $\lambda_{\lim}^2 \sim 2gd_1/9\omega_1^2$. Thus for $\Omega_1 \gg 1$, $\lambda_{\lim}/h_{\lim} \sim \omega_1(2gd_1)^{1/2}/72g$. Hence we would not expect a solution that scales with $h_{\lim}$ as $\Omega_1 \to \infty$.

With $\Omega_1 = -1.1125$, -1.25, and 1.50 we encountered difficulties using the Q_1 parametrization scheme at values of $A = 4.46$, $A = 6.19$, and $A = 12.64$, respectively, although we were unable to determine the reason for this. However, no such difficulty was encountered using the σ parametrization scheme, and the solution branches shown in Figs. 2 and 4 were calculated using this scheme. For $\Omega_1 \lesssim -1.125$ we found solutions corresponding to waves of very large amplitude. One such sequence for $\Omega_1 = -1.50$ is shown in Fig. 4. We speculate that these results may indicate a change in the character of the limiting wave from a shape characterized by a 120° corner at the wave crest to a bubble-capped wave, where the bubble dimension increases rapidly with $-\Omega_1$. Some properties of these very-large-amplitude waves have been investigated independently by Teles da Silva and Peregrine[12] for long periodic surface waves in the presence of uniform vorticity.

In Fig. 5 we show the total excess energy E [i.e., $E = T + V$, see (11a) and (11b)] for $-1.5 \leqslant \Omega_1 \leqslant 0$. When $\Omega_1 > 0$ we found waves with $E < 0$, and these waves are not shown on the log scale of Fig. 4. Generally for all values of Ω_1 used here, the first maximum in E appears to occur at slightly smaller values of A than the first maximum in C. Also log-linear plots of the wave profile showed that for all values of Ω_1 treated, the wave tails had exponential decay as $|X| \to \infty$ as expected.

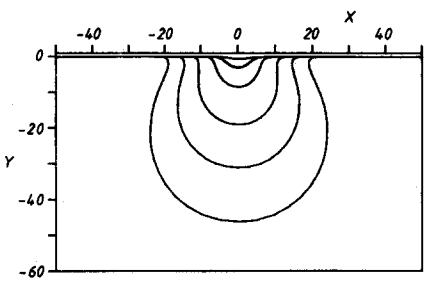

FIG. 4. A sequence of wave profiles for free-surface solitary waves on a uniform shear flow; $\alpha = -1$, $\Omega_1 = -1.50$. Here gravity acts in the positive Y direction.

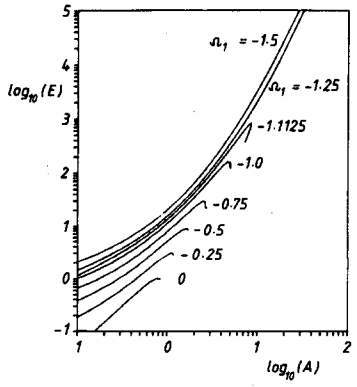

FIG. 5. Total excess wave energy E versus wave amplitude A for free-surface solitary waves on a uniform shear flow; $\alpha = -1$, and values of Ω_1 indicated.

B. Interfacial solitary waves: $-1 < \alpha < 1$

Here we report calculations in the range $-1 < \alpha \leq 0.2$ performed using the σ parametrization. The solution procedure followed was essentially the same as for the free-surface waves described in Sec. V A, except that here we put $\Omega_1 = 0$, and track solutions on branches where α is a constant. In Fig. 6 we show a sequence of wave profiles near the crest for extreme waves, each for a fixed value of α near $\alpha = -1$. When $\alpha = -0.9$ and $\alpha = -0.925$, the extreme wave profiles indicate a limiting wave in which distinct portions of the interface profile touch forming a bubble of stagnant fluid density ρ_1. Limiting waveforms of this type were suggested by Meiron and Saffman[17] for periodic waves, and evidence supporting this conjecture was given by Grimshaw and Pullin[18] for the Boussinesq limit, $\alpha \to 0$. The extreme wave profiles found here for $\alpha = -0.95$, -0.975, and -0.99 do not show an overhanging profile, and there is no firm indication of a bubble-capped limiting wave. However, we suspect that this is due to difficulties with numerical resolution associated with a rapid variation of the solution as $\delta \to \delta_{\text{lim}}$ and $\alpha \to -1$ simultaneously. We note that when $D_2 \to \infty$ the limit $\alpha \to -1$ is necessarily singular, as the inertia and energy of the lower fluid (with density $1 + \alpha$) is infinite for arbitrarily small values of $1 + \alpha$, but must vanish when $\alpha = -1$. We

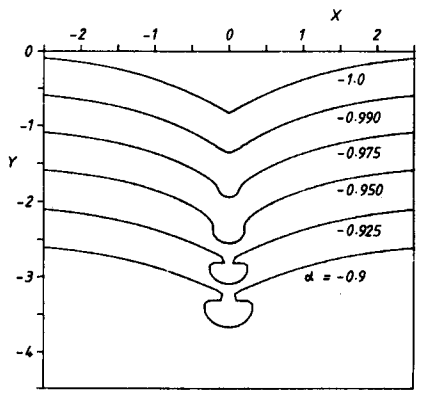

FIG. 6. Extreme wave profiles near the crest for interfacial solitary waves; $\Omega_1 = \Omega_2 = 0$ and values of α indicated. Only the profile with $\alpha = -1$ is at the correct Y level, while the other profiles are successively displaced 0.5 units in the negative Y direction. Here gravity acts in the positive Y direction.

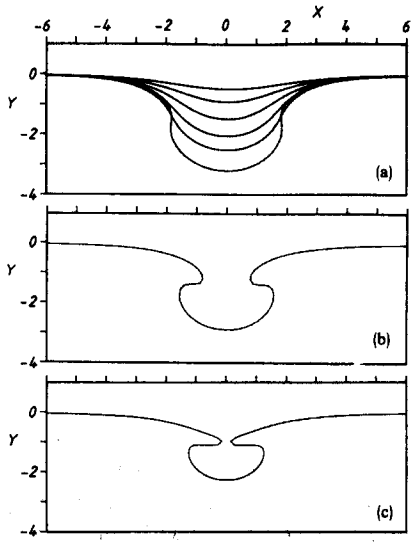

FIG. 7. Wave profiles for interfacial solitary waves; $\alpha = -0.7$, $\Omega_1 = \Omega_2 = 0$. Here (a) is a family of waves with increasing wave amplitude A; (b) is an overhanging wave; (c) is an extreme wave. Here gravity acts in the positive Y direction.

conjecture that all solution branches with α constant, at a value near $\alpha = -1$, are terminated by a bubble-capped wave, and that the bubble dimension vanishes as $\alpha \to -1$. We also found that the maximum allowable A_{ex}, for a fixed value of α, decreased monotonically as $\alpha \to -1$, in agreement with the results of Holyer[13] for periodic interfacial gravity waves in unbounded fluids ($D_{1,2} \to \infty$).

In Figs. 7–9 we show sequences of wave profiles for $\alpha = -0.7$, -0.5, and -0.3, respectively (see also Fig. 10). The progression toward a bubble-capped limiting profile is again evident, although for the case $\alpha = -0.3$ the extreme wave found is well short of the conjectured limiting wave, because of numerical resolution difficulties with $N = 40$. The first appearance of overhanging on the wave profile appears to be associated with a turning point in the

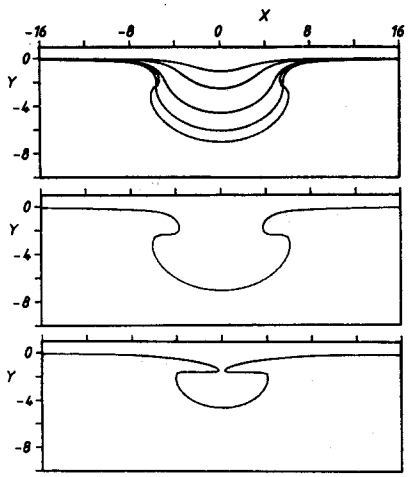

FIG. 8. Wave profiles for interfacial solitary waves; $\alpha = -0.5$, $\Omega_1 = \Omega_2 = 0$.

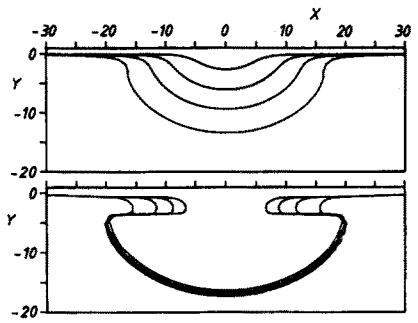

FIG. 9. Wave profiles for interfacial solitary waves; $\alpha = -0.3$, $\Omega_1 = \Omega_2 = 0$.

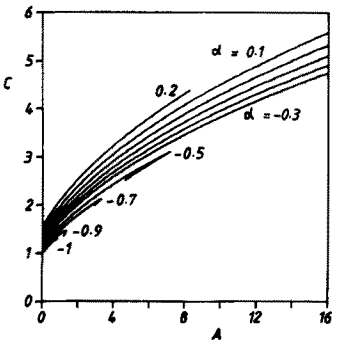

FIG. 11. Wave speed C versus wave amplitude A for interfacial solitary waves; $0.2 > \alpha > -1$, $\Omega_1 = \Omega_2 = 0$, and values of $\alpha = 0.2$ to $-0.3(-0.1)$, -0.5, -0.7, -0.9, and -1.0.

graph of C vs A, which can be seen on a very small scale in Fig. 11 when $\alpha = -0.9$, -0.7, and -0.5. When $\alpha = -0.2$, -0.1, 0, and 0.1, wave profiles with very large values of A were found. With $\alpha = -0.2$, overhanging first occurred when $A \approx 44.63$ and with $\alpha = -0.1$, at $A \approx 160$, but further calculations on these branches were not possible because of degrading resolution with $N = 40$. In Fig. 10 we show a sequence of wave profiles for the case of the Boussinesq limit, $\alpha = 0$. In Fig. 11 we show the speed C as a function of amplitude A for a sequence of values of α. Note the trend toward very large amplitudes as $\alpha \to 0$, and the presence of turning points. As we commented above the failure to find turning points on some branches with a low value of α is probably a result of lack of resolution in the numerical solutions when A is very large.

In Fig. 12 we plot the wave profiles on a log–log scale for the case $\alpha = 0$ in order to obtain information on the decay of the wave tail. For moderate values of A ($A < 10$) the near tail appears to decay as X^{-2} in agreement with the analytical predictions for the limit $A \to 0$ (see Benjamin[6] and Davis and Acrivos[7]), but the far tail shows decay like X^{-4} even at the smallest amplitude displayed. While this may be the effect of numerical truncation errors accentuated by the presence of the singularity at $\zeta = -1$, calculations at other values of α did appear to show a weak dependence of the tail structure with α when $\alpha \to -1$. For example, results at $\alpha = -0.9$ with $N = 40$ and $N = 60$ both indicate uniform decay of the tail like X^{-3} with no X^{-2} or X^{-4} region. Hence it seems possible that the far tail behavior of Fig. 12 is a genuine finite-amplitude effect.

C. Boussinesq limit: $\alpha = 0$

The ease with which we obtained numerical solutions for $\alpha = 0$ with very large values of amplitude A suggests that solitary waves in this case may be of unbounded amplitude. This is supported by the shape of the calculated wave profiles shown in Fig. 10. For $A \gg 1$ the profiles are similar in shape and appear to differ only by a scale factor. This hypothesis was tested numerically by replacing the conformal mapping (19) by

$$\zeta = \{[Z + i(1 - D_1)]/[Z - i(1 + D_1)]\}, \qquad (38)$$

so that D_1 is a parameter in the numerical scheme. The integral equation formulation using (37) in place of (19) proceeds in a manner analogous to that described in Sec. III. We then, with $\alpha = 0$, took a solution from the case $D_1 = 1$ and determined a corresponding value of amplitude A. With A then fixed at this value, we successively reduced D_1 in small increments from $D_1 = 1$ to $D_1 = 0$. When $D_1 = 0$ we note that (38) maps the lower and upper halves of the Z plane into the interior, respectively, of the unit circle in the ζ plane, while the rigid boundary becomes $Y = 0$. Since the solution "feels" D_1 only through (38), together with the image effect of L in the rigid boundary, letting $D_1 \to 0$ with A fixed is equivalent to letting $A \to \infty$ with D_1 fixed. In effect we are choosing the length scale H (see the beginning of Sec. III) to be the wave amplitude.

The wave profile obtained using this procedure, with $N = 80$, is shown in Fig. 13, scaled so that $A = 1$. The profile displacement is finite only in $|X| < 2.18$, since for $|X| > 2.18$,

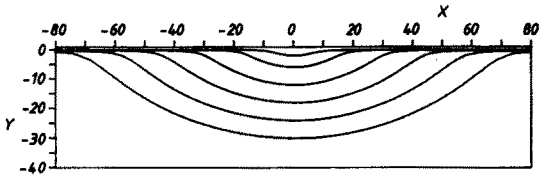

FIG. 10. Wave profiles for interfacial solitary waves; $\alpha = 0$, $\Omega_1 = \Omega_2 = 0$. Here gravity may act in either direction.

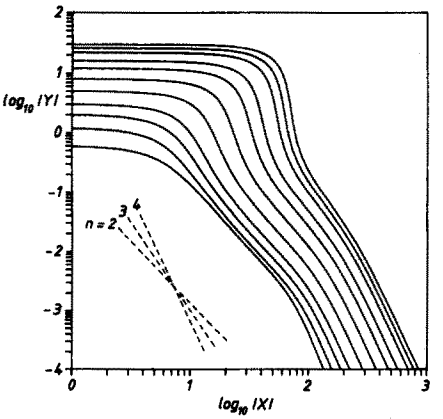

FIG. 12. Partial wave profiles for interfacial wave profiles; $\alpha = 0$, $\Omega_1 = \Omega_2 = 0$. Here --- indicates the slope of the curve $Y = (\text{const})\, X^{-n}$.

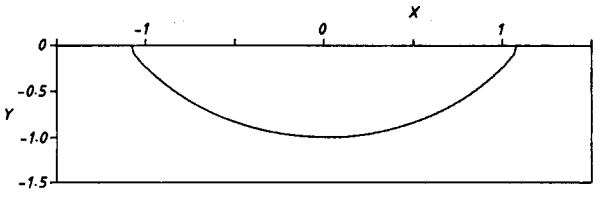

FIG. 13. The limiting wave profile for an interfacial solitary wave; $\alpha = 0$, $\Omega_1 = \Omega_2 = 0$, $D = 0$, and $A = 1$.

$|Y|$ is $O(10^{-10})$. This indicates that as $A \to \infty$ with D_1 fixed, the limiting wave has a half-lens shape of approximate dimensions $4.36A \times A$, which encloses a stagnant bubble of fluid. At the two stagnation points $X = \pm 2.18$, $Y = 0$, a local analysis shows that the limiting profile must intersect the X axis at 120°. Since the flow in this corner was not well resolved locally by our finite difference method, there is some irregularity in the profile of the wave tails which can be seen in Fig. 13.

With $A = 1$, we obtain $C = 1.30$ and $E = 3.30$ for the limiting wave $D_1 \to 0$. When $A \to \infty$ with D_1 fixed, dimensional analysis based on the equivalence of the limits $A \to \infty$, $D_1 = 1$, and $A = 1$, $D_1 \to 0$ shows that C is proportional to $A^{1/2}$ while the total energy E is proportional to A^3. Hence, in the limit $A \to \infty$ with $D_1 = 1$,

$$C \sim 1.30A^{1/2}, \quad E \sim 3.30A^3. \tag{39}$$

These results agree well with the behavior of C (Fig. 11) and E (calculated but not displayed) at large values of A. In dimensional terms, $c \sim 1.30\,(\alpha g h)^{1/2}$, $\hat{E} \sim 6.60 \rho \alpha g h^3$ where h, c, and $\hat{E}$ are the dimensional wave amplitude, speed, and energy, respectively. Finally by plotting A_{ex} against $|\alpha|$ on a log–log scale, our calculations with α in the range $-0.5 \leqslant \alpha \leqslant 0$ suggest that $A_{ex} \sim 1.55\alpha^{-2}$ as $\alpha \to 0$, with $\alpha < 0$.

ACKNOWLEDGMENT

The contribution of D. I. Pullin to this work was supported by the Australian Research Grants Scheme under Grant No. A48315031.

[1] J. W. Miles, Annu. Rev. Fluid Mech. **12**, 11 (1980).
[2] R. Grimshaw, *Encyclopedia of Fluid Mechanics* (Gulf, Houston, TX, 1986), Vol. 2, I, Chap. 1, p. 3.
[3] J. K. Hunter and J. M. Vanden-Broeck, J. Fluid Mech. **136**, 63 (1983).
[4] G. G. Stokes, *Mathematics and Physics Papers* (Cambridge U.P., Cambridge, 1905), Vol. 5, p. 163.
[5] G. H. Keulegan, J. Res. Nat. Bur. Stand. **51**, 133 (1953).
[6] T. B. Benjamin, J. Fluid Mech. **29**, 559 (1967).
[7] R. E. Davis and A. Acrivos, J. Fluid Mech. **29**, 593 (1967).
[8] R. J. Joseph, J. Phys. A: Math. Nucl. Gen. **10L**, 225 (1977).
[9] C. J. Amick and R. E. L. Turner, Trans. Am. Math. Soc. **298**, 431 (1986).
[10] M. Funakoshi and M. Oikawa, J. Phys. Soc. Jpn. **55**, 128 (1986).
[11] J. Simmen and P.G. Saffman, Stud. Appl. Math. **73**, 35 (1985).
[12] F. Teles da Silva and D. H. Peregrine, submitted to J. Fluid. Mech.
[13] J. Holyer, J. Fluid Mech. **93**, 433 (1979).
[14] J. M. Vanden-Broeck, Phys. Fluids **23**, 1723 (1980).
[15] D. I. Pullin and R. H. J. Grimshaw, Phys. Fluids **26**, 897 (1983).
[16] D. I. Pullin and R. H. J. Grimshaw, Phys. Fluids **26**, 1731 (1983).
[17] D. I. Meiron and P. G. Saffman, J. Fluid Mech. **129**, 213 (1983).
[18] R. H. J. Grimshaw and D. I. Pullin, Phys. Fluids **29**, 2801 (1986).
[19] R. E. L. Turner and J. M. Vanden-Broeck, Phys. Fluids **29**, 372 (1986).
[20] M. S. Longuet-Higgins, Proc. R. Soc. London Ser. A **337**, 1 (1974).
[21] J. A. Zufiria, J. Fluid Mech. **181**, 17 (1987).
[22] J. A. Zufiria, J. Fluid Mech. **180**, 371 (1987).
[23] J. A. Zufiria, J. Fluid Mech. **184**, 183 (1987).
[24] H. B. Keller, in *Applications of Bifurcation Theory* (Academic, New York, 1977), p. 359.
[25] M. Tanaka, Phys. Fluids **29**, 650 (1986).